ARTICLE NO. 78-497

Numerical and Experimental Comparison of the Notch Tip Stresses in a Laminated Plate

W. P. Witt III* and A. N. Palazotto†
Air Force Institute of Technology, Wright-Patterson Air Force Base, Ohio
and
H. T. Hahn‡
Air Force Materials Laboratory, Wright-Patterson Air Force Base, Dayton, Ohio

A crack in a laminated, composite plate was modeled using numerical methods. The experimental results used to validate this analysis were for a $(0, \pm 45, 90)_s$ graphite-epoxy plate with a center notch oriented normal to the loading direction. Two two-dimensional finite-element models were used to determine the size of the crack tip damage zones. One involved a purely elastic analysis; in the other, the element ply stiffness was completely discounted if the stresses exceeded the Tsai-Hill failure criterion. Diagrams showing the growth and shape of the ply damage zones at increasing load levels were developed for both models. The size of the subcracks in each ply were linearly related to the opening-mode stress intensity factor K_I. A critical stress intensity factor approach, an instability approach, and a new fracture load prediction method based on load-vs-load-bearing-area diagrams were used to predict the fracture load. Since this new method provided close upper and lower limits on the fracture load and is possibly applicable to complicated structures, it was considered the best of the three methods.

Introduction

THIS paper is specifically concerned with the use of numerical methods to model a crack in a laminated graphite-epoxy composite plate. The crack is simulated by a through-the-thickness, finite-width center notch oriented normal to the loading axis. Conventional finite-element analysis and classical laminated plate theory are used in the numerical model. These techniques are coupled with the use of composite strength theory and incremental loading to follow the growth and development of the damage zone at the crack tip and eventually determine a failure load.

At the present time, the direct applicability of LEFM to laminated composite fracture cannot be assumed.[1-3] The presence of notch sensitivity[1] and the fact that crack growth parallel to the fibers in unidirectional composites can be explained by a stress intensity factor[4,5] indicate that some portions of presently developed isotropic fracture theory can be applied. The major divergences from isotropic fracture theory are the growth of a damage zone as opposed to crack opening from the crack tip and the dissimilar behavior of each ply in a laminate to a given load.

The data that will be used to validate the analysis done in this paper were generated by the Air Force Materials Laboratory.[6,7] During the experiments, notched composite plates of Thornel 300 graphite fibers in Narmco 5208 were loaded to failure. The specimens contained a 13-mm notch in $(0, \pm 45, 90)_s$ laminate. As part of these experiments, radiographs were taken at various load levels. The radiographic image of the crack tip damage area was enhanced.[8] From these radiographs, it was then possible to measure the length of the subcracks in each ply of the laminate.

Received March 8, 1978; presented as Paper 78-497 at the AIAA/ASME 19th Structures, Structural Dynamics and Materials Conference, Bethesda, Md., April 3-5, 1978; revision received Nov. 20, 1978.

Index category: Structural Composite Materials.

*Ph.D Candidate, Aeronautics and Astronautics Dept. Associate Member AIAA.

†Professor, Aeronautics and Astronautics Dept. Member AIAA.

‡Research Engineer; presently at Lawrence Livermore Laboratories, Livermore, Calif.

Theory

Several investigators have stated that the stress field around a crack in a composite plate is three dimensional.[2,3,9] The three dimensionality is caused by the interlaminar stresses at the free edge of a crack. In Ref. 10, the effects of interlaminar stresses on the fracture strength of center notched graphite-epoxy laminated plates were studied experimentally. This study showed that the stacking sequence, and hence the interlaminar stresses, had no effect on the fracture strength of a center-notched plate. Thus, it seems feasible to use a two-dimensional analysis to model the boundary of the damage zone for the problem considered.

In general for any material, strength is a measure of the ability to deform without sustaining irreversible damage. In homogeneous isotropic materials, this ability is measured by the yield criterion, where the yield strength is the point where the material ceases to act elastically. Drawing a parallel with plasiticity theory, it can then be surmised that the combinations of stresses that cause lamina failure can be represented by a hypersurface in stress space.[5] Lamina failure is defined as the inability of the lamina to carry stress in the same manner it did in its virgin state. To determine when this inability occurs, the Tsai-Hill failure criterion[11,12] will be used with the failure strength parameters determined from the uniaxial strengths for the two-dimensional case such that the criterion becomes

$$\frac{\sigma_1^2}{X^2} - \frac{\sigma_1\sigma_2}{X^2} + \frac{\sigma_2^2}{Y^2} + \frac{\sigma_{12}^2}{S^2} = 1 \tag{1}$$

where X is axial strength, Y transverse strength, and S shear strength.

Before this criterion can be applied to a laminate, a determination must be made as to how to treat constituent lamina failure when it occurs prior to total laminate failure. After putting laminae together to form a laminate, the behavior of the laminate is no longer linear to failure. Instead it can be assumed that failure of the laminate occurs when all of its constituent laminae have failed.[5,9] There are basically three methods to modify the laminate stiffness after lamina failure[5]: the total discount method; where the failed ply is assigned zero stiffness and strengths; the mode limited

discount method; and the method in which residual properties are assigned to the failed lamina.

Since the exact lamina failure mechanisms and the post-failure performance of the laminae in a laminate are not completely understood, this analysis uses a bounding argument to portray failure in the crack tip damage zone. It is obvious that one extreme bound on the damage zone can be found if all laminae are treated as elastic until failure occurs (elastic method); the other extreme bound is determined by completely discounting all stiffness of a ply when the stress field in that ply exceeds the failure criterion (progressive failure method).

The appropriateness of two-dimensional analysis, the Tsai-Hill failure criterion, the progressive lamina failure approach to predict laminate failure, and the boundedness assumption made in the analysis were checked by applying these procedures to an unnotched specimen under tension. The properties of the graphite-epoxy specimen used are shown in Table 1. Using the methods described, the elastic model provides an upper bound, and the progressive failure model provides a lower bound on the actual failure load.

The goal of a fracture analysis is to predict in what fashion and when catastrophic failure will occur. The manner of failure can be correlated with either crack propagation or the growth of a damage zone at the crack tip. The "when" of ultimate failure is explained by the fracture stress if time-related phenomena are ignored. The phenomena correlated with these two questions will be discussed in the following paragraphs.

Since crack extension did not occur for the tests being analyzed, the investigation must concentrate on explaining the growth of the damage zone. Two specific phenomena are related to the growth of the damage zone. The unobservable phenomenon is the growth of the failure area around the crack tip. This phenomenon is measured using strength theory, as explained previously. The observable occurrence is the growth of subcracks along ply fibers.[1,3] Ultimately, it should be possible to relate the growth of these subcracks and the remaining safe life of the structure in a manner similar to that described in Ref. 13. First, the relation between the growth of subcracks and the fracture strength must be investigated. Although it is questionable whether the growth of subcracks and the fracture stress are directly related,[1] it has been shown that the length of the subcracks is proportional to the opening-mode stress intensity factor squared $(K_I)^2$ (Ref. 1). The average length of the ply subcracks can be obtained experimentally from radiographs of the crack tip damage zone, while values of K_I can be found from the finite-element analysis results and the following expression for a center-notched, finite-width plate[14]:

$$K_I = \sigma[w\tan(\pi a/w)]^{1/2} \tag{2}$$

In this expression, σ is the applied stress, w is the plate width, and a is the effective crack half-length. The effective crack half-length is the sum of the original crack half-length a_o and the size of the damage zone c, measured collinear with the original notch:

$$a = a_o + c \tag{3}$$

Table 1 Lamina properties

Elastic constants	Ultimate strengths (ksi)
Thickness, $t = 0.0054$ in.	$X_t = 217.6$
Longitudinal modulus, $E_{11} = 15545$ ksi	$S_c = 217.6$
Transverse modulus, $E_{22} = 1425$ ksi	$Y_t = 5.8$
Shear modulus, $G_{12} = 903$ ksi	$S = 9.9$
Poisson's ratio, $\nu_{12} = 0.288$	$(0, \pm 45, 90)_s = 54.4$

The methodology used to determine c will be explained later.

The prediction of when fracture occurs can be approached in three manners. Two of these, the use of a critical stress intensity factor and instability analysis are classical in nature, and the third is introduced, for the first time, in the paper. The third involves the relation between combinations of load and load-bearing area.

The use of stress intensity factors is well described in many articles on fracture mechanics and will not be discussed herein. The instability method of predicting fracture strength is the simplest to apply. The load-displacement curve for the sequence of loading, where element plies within the failure region are removed, is plotted. The increment of the load that causes the curve to transition from the nonlinear region to the flat region is defined as the instability load, and the preceding load is taken as the fracture strength.

The third and newly developed method is based on logic similar to that presented in an article by Nuismer and Whitney.[15] The average stress criteria predicts failure when the average value of stress σ_a, over some fixed distance d_0, ahead of the crack first reaches the unnotched tensile strength, σ_0. In equation form, failure occurs when

$$(d_0)^{-1}\int_a^{a+d} \sigma_x(0,y)\,dy = \sigma_0 \tag{4}$$

where d_0 is the fixed distance ahead of the crack, a is the crack length, and σ_x is the normal stress component ahead of the crack tip. For this type of specimen it can be shown that this relation becomes

$$P_{ax}/A_{LB} = \sigma_0 \tag{5}$$

where A_{LB} is the remaining undamaged load-bearing area and P_{ax} is the applied load in the x direction.

To find the fracture strength for a particular material, Eq. (5) is applied to a load-vs-load-bearing-area diagram. The boundary of the failure region is the line defined by

$$P/A = \sigma_0 \tag{6}$$

As damage progresses from the crack tip, the load-bearing area decreases. If load and remaining load-bearing area are plotted, the predicted fracture strength is the intercept between this curve and the boundary of the failure region. Referring to the boundedness argument presented previously, the elastic method yields an upper bound on strength, and the complete discount method yields a lower bound.

Numerical Analysis

The finite-element program used in this paper was developed at the Air Force Flight Dynamics Laboratory.[16] The program is based on classical laminated plate theory and the displacement method of finite-element analysis. This program could be used to analyze plies of several different combinations, one of which was $(0, \pm 45, 90)_s$, and included various standard elements, including the constant-strain triangle. The element stiffness matrix is modified by either changing the relative percentage of the plies contained in the element laminate or by changing the element material.

For this analysis two finite-element meshes were generated making use of the information presented in Ref. 17. In the first, with 163 nodes and 282 elements, the ratio of element area to squared crack length, A_E/a^2, was approximately 20×10^{-6}. In the second, shown in Fig. 1, with 252 nodes and 457 elements, the A_E/a^2 ratio was 10×10^{-6}. The accuracy and convergence of these two meshes when applied to the composite crack problem was shown to be acceptable.

There are two general procedures that are followed in the numerical analysis stage. One is for the purely elastic method,

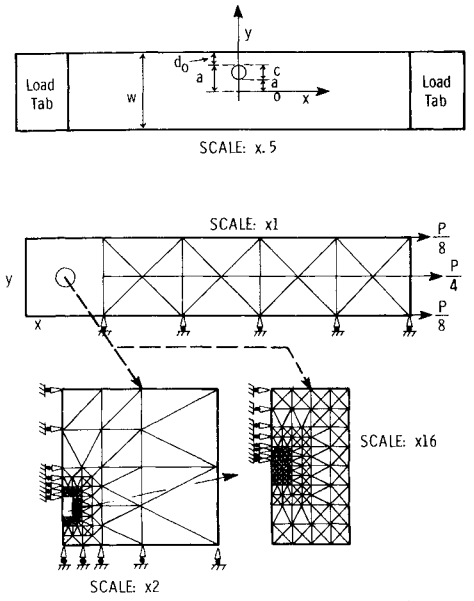

Fig. 1 Second mesh 252 nodes, 457 elements.

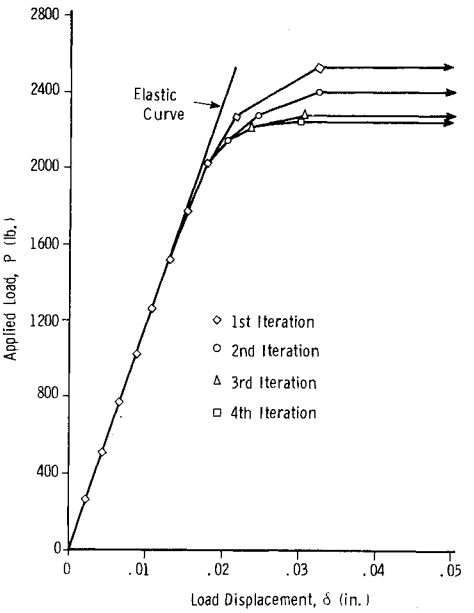

Fig. 2 Load vs displacement curve for progressive failure model.

and the other is for the method that employs ply removal. In the elastic method, loads are applied in increments of 10% up to the experimentally determined strength. At each level of loading, the bounds of the damage zone are determined, but the element stiffnesses are not changed. In the method using ply removal, the same general procedure is initially followed, but after each increment of loading the element plies that failed are removed before the next increment of load is applied. When using ply removal, a method similar to Chou et al.[18,19] is incorporated. They were interested in employing ply stiffness reduction through experimental properties, as opposed to the technique advanced herein where all ply stiffness is removed. If the displacement at the load application point differs by more than 10% for the same load, the load increment is halved until the model converges. This procedure is continued until either the experimentally determined strength is reached or the model becomes unstable, with instability defined by the point where the slope changes by more than a factor of 50.

Results

The load-displacement curves for the elastic and the progressive failure models are shown in Fig. 2. Four iterations were required before the progressive failure model converged. The last iteration started at 87.5% of the experimental fracture strength and developed an instability at 90%.

The damage zone diagrams for three representative load levels for the elastic model are shown in Figs. 3-5. The plots correspond to the portion of the plate shown in the figures. The coordinates x and y are normalized by dividing them by the plate width w. The dotted line parallel to the y axis represents the crack, and the crack tip is located at $y/w = 0.13$. The boundary of the plate is at $y/w = 0.5$.

Several generalizations can be drawn from examinations of the plots. First, the damage zone remains very small until 40% of the fracture strength is reached. In the diagram for 80% of the fracture strength, the general shape of the damage zones in each ply can be seen.

The damage zone in each ply generally extends the farthest in a direction perpendicular to the fiber direction. This is caused by the large amount of shearing and transverse failure. The damage zone extends slightly behind the crack tip in all plies.

The 90-deg ply has the largest damage zone, and the zone in this ply grows the fastest. At 100% of the fracture load, all of the 90-deg ply has failed except for a small area along the crack flanks.

The boundaries for the +45 and −45-deg plies essentially coincide. The small deviances that occur are believed to be caused by numerical approximation. The stress fields in the ±45-deg plies have shown the greatest disparity among adjoining elements and thus an averaging technique was employed.[20]

The smallest damage zone is that for the 0-deg plies. As can be seen, it is narrow and pointed. The area bounded by the 0-deg damage zone is also the area in which all plies have failed and is represented by the damage zone's dimension c, presented in Table 2. The damage zone dimension is measured from the tip of original crack to the tip of the 0-deg damaged zone in the direction of the original crack. It must be recognized that other plies have been damaged outside of this zone, but the plate still retains some load-carrying capacity. The growth of this zone simulates crack growth.

The damage zone boundaries for the progressive failure model are shown in Figs. 6-8. The boundaries for the elastic model and the progressive failure model are similar up to the 50% load level. At this point, the damage zones in the progressive failure model begin to grow faster. Another dissimilarity is that the growth of the damage zone behind the crack tip stops at 50%. The removal of element plies creates

Table 2 Damage zone dimensions (calculated from finite element)

Applied stress, ksi	Elastic model c, in.	Progressive failure model c, in.
2.98	0.0	0.0
5.88	0.0	0.0
8.86	0.008	0.006
11.84	0.013	0.014
14.73	0.019	0.032
17.72	0.026	0.065
20.61	0.031	0.121
23.59	0.037	0.193
25.09	—[a]	0.314
25.83	—[a]	0.507
26.20	—[a]	0.728
26.58	0.048	—[a]
29.47	0.056	—[a]

[a] Analysis was not performed for these loads.

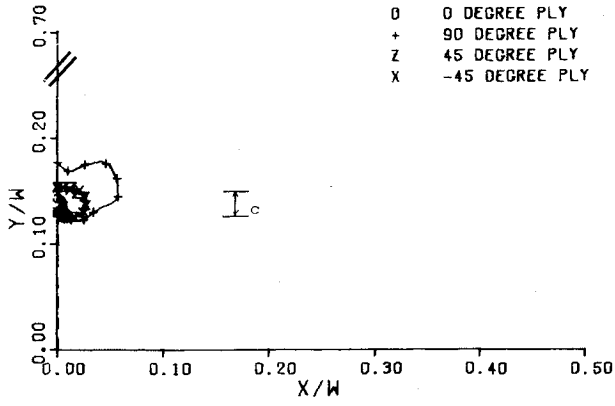

Fig. 3 Damage zone prediction at 60% of experimental fracture load, using elastic model.

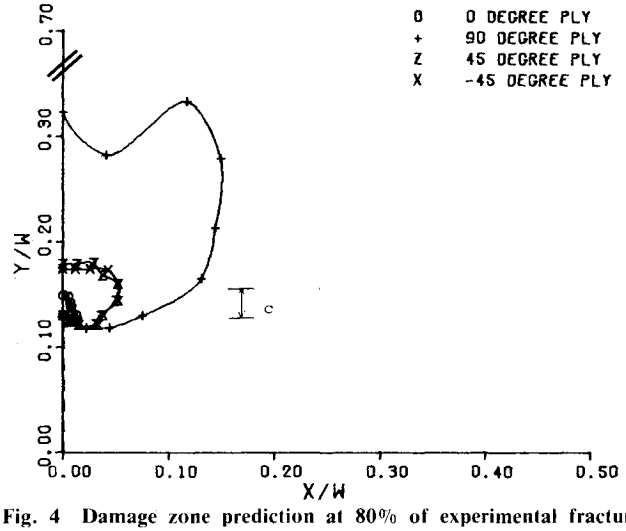

Fig. 4 Damage zone prediction at 80% of experimental fracture load, using elastic model.

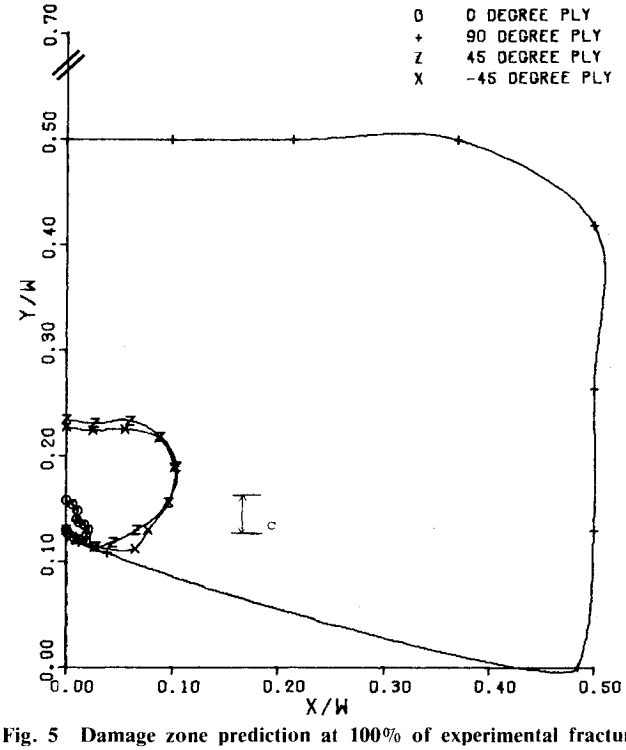

Fig. 5 Damage zone prediction at 100% of experimental fracture load, using elastic model.

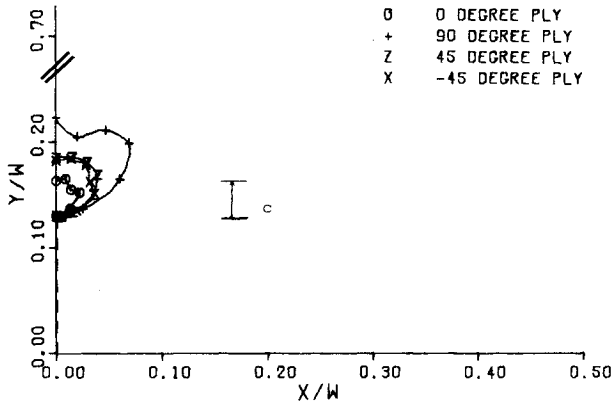

Fig. 6 Damage zone prediction at 60% of experimental fracture load, using progressive failure model.

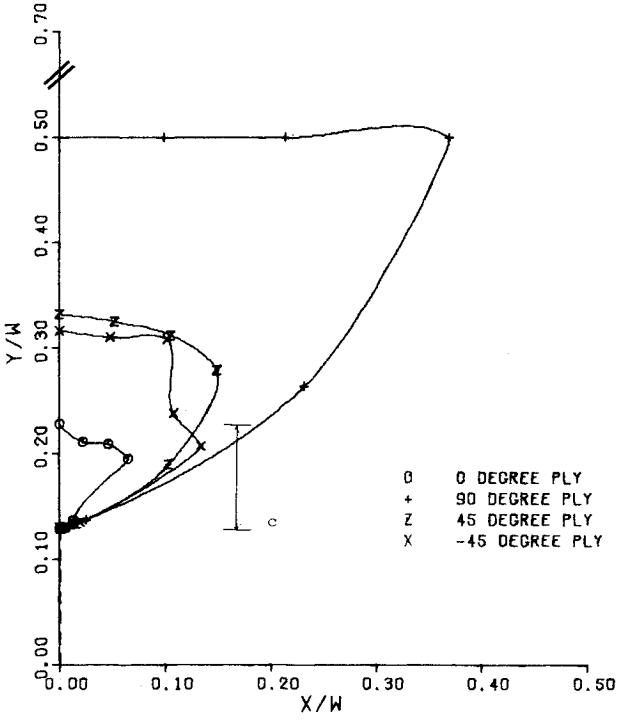

Fig. 7 Damage zone prediction at 80% of experimental fracture load, using progressive failure model.

an equivalent free edge stress similar to the stresses exhibited along the crack flanks.

At the 85% load level, the ±45-deg plies and the 90-deg ply have failed in the entire region between the crack tip and the edge of the plate. Contrary to what happens with the elastic model, the 90-deg ply never fails over the entire plate. Ultimate failure becomes imminent when 0-deg ply damage zone reaches the edge of the plate at 88.75% of the experimental fracture strength.

The first application of the finite-element analysis is to check the correlation between the experimental subcrack lengths in each ply and the numerical values of $(K_I)^2$. Two values of K_I are calculated; one is for the purely elastic analysis, and the other is for the progressive failure analysis.

The first task is to determine the length of the ply's subcracks. The subcrack measurements are obtained from the radiographs. The measurements were made from the crack tip in each ply's fiber direction. Subcrack lengths, shown in Table 3, are the average of the measured lengths.

The values of K_I are obtained from Eqs. (2) and (3). The crack half-length a is calculated using Eq. (3). The computed

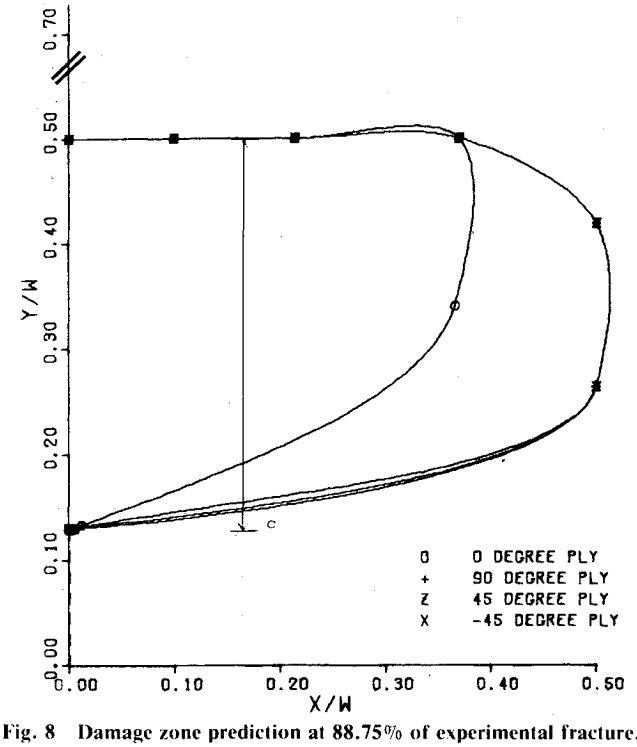

Fig. 8 Damage zone prediction at 88.75% of experimental fracture, load, using progressive fracture model.

Table 3 Subcrack lengths (measured)

Applied stress, ksi	0-deg ply, in.	90-deg ply, in.	±45-deg ply, in.
14.734	0.031	0.047	0.023
17.718	0.055	0.086	0.039
20.609	0.057	0.115	0.046
23.593	0.060	0.226	0.068
26.577	0.084	0.436	0.092
28.069	0.087	0.564	0.095

Table 4 K_I calculations (elastic model)

Applied stress, ksi	Half-crack length, in.	Plate width, in.	K_I ksi-in.$^{1/2}$	$(K_I)^2$, ksi^2-in.
2.98	0.256	1.97	2.75	7.59
5.88	0.256	1.97	5.00	25.04
8.86	0.264	1.97	8.32	69.24
11.84	0.269	1.97	11.04	121.85
14.73	0.274	1.97	14.15	200.19
17.72	0.281	1.97	17.28	298.44
20.61	0.287	1.97	20.28	411.36
23.59	0.293	1.97	23.51	552.87
26.58	0.303	1.97	27.04	731.34
29.47	0.312	1.97	30.46	927.85

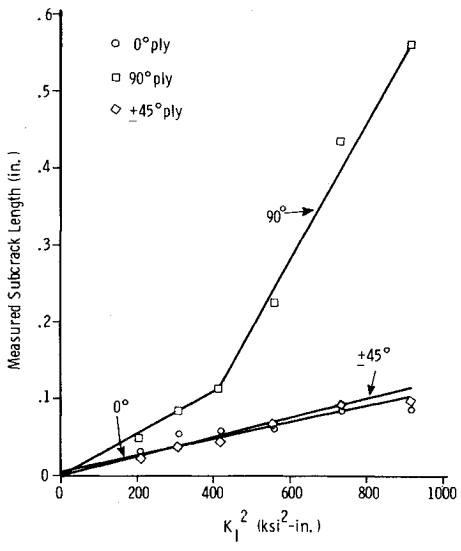

Fig. 9 $(K_I)^2$ vs subcrack length for elastic model.

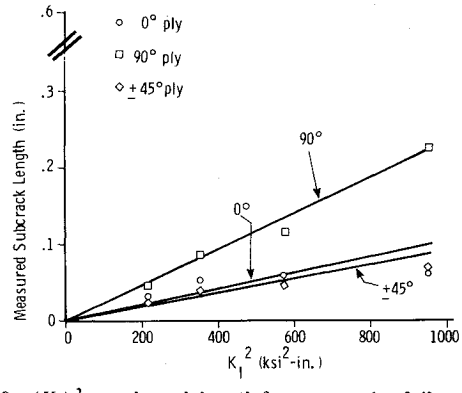

Fig. 10 $(K_I)^2$ vs subcrack length for progressive failure model.

Table 5 K_I calculations (progressive failure model)

Applied stress, ksi	Half-crack length, in.	Plate width, in.	K_I ksi-in.$^{1/2}$	$(K_I)^2$, ksi^2-in.
2.98	0.256	1.97	2.75	7.59
5.88	0.256	1.97	5.00	25.04
8.86	0.262	1.97	8.28	68.50
11.84	0.270	1.97	11.27	126.98
14.73	0.288	1.97	14.55	211.62
17.72	0.321	1.97	18.65	344.93
20.61	0.377	1.97	23.96	573.85
23.59	0.449	1.97	30.89	953.51
25.09	0.570	1.97	39.89	1591.36
25.83	0.463	1.97	59.66	3558.77
26.20	0.984	1.97	4115.75	16.9×10^6

values of K_I at the various stress levels for the elastic analysis are shown in Table 4.

The values of K_I for the progressive failure analysis are shown in Table 5. This table does not go to the same stress level as the elastic analysis, since the analysis developed an instability before 100% of the experimental notched strength was reached.

The values of $(K_I)^2$ determined from the elastic analysis vs the subcrack length in each ply are shown in Fig. 9. As was found in Ref. 1, there appears to be a linear relation between $(K_I)^2$ and the subcrack lengths.

The values of $(K_I)^2$ determined from the progressive failure analysis vs subcrack lengths are shown in Fig. 10. For the values of $(K_I)^2$, considering values of load from 14.7341 to 23.593 ksi, the correlation appears to be linear. At the last load level, where the damage zone extends to the edge of the plate, there is no correlation between $(K_I)^2$ and the subcrack lengths.

As was stated previously, calculated values of the opening-mode stress intensity factor K_I can be used to predict failure. For this specimen the critical stress intensity factor[6] is between 40.22 and 41.67 ksi-in.$^{1/2}$. Referring to Table 4, it is seen that failure would occur at some value over 29.47 ksi, which is the experimental notched strength. If the value of K_I continued to increase in the same manner, the predicted fracture strength would be approximately 39 ksi or 32% over

Table 6 Load and load bearing area data

Load P lb	Elastic A_{LB} in.^{2}	Progressive failure A_{LB} in.^{2}
256	6.35×10^{-2}	6.35×10^{-2}
504	6.35×10^{-2}	6.35×10^{-2}
760	6.28×10^{-2}	6.30×10^{-2}
1016	6.24×10^{-2}	6.22×10^{-2}
1264	6.19×10^{-2}	6.07×10^{-2}
1520	6.12×10^{-2}	5.78×10^{-2}
1768	6.08×10^{-2}	5.29×10^{-2}
2024	6.03×10^{-2}	4.67×10^{-2}
2152	—[a]	3.61×10^{-2}
2216	—[a]	1.93×10^{-2}
2248	—[a]	0
2280	5.93×10^{-2}	—[a]
2528	5.86×10^{-2}	—[a]

[a] Analysis was not performed for these loads.

the experimental strength. Using the values of $(K_I)^2$ in Table 5, the failure strength would be between 25.09 and 25.83 ksi. This is in error by 12-15%. As was expected, the elastic analysis provides an upper bound on the fracture strength and the progressive failure analysis provides a lower bound.

The load-displacement diagram, Fig. 2, can be used to determine the fracture load from a stability standpoint. After the last iteration the slope changes from 5.104×10^3 lb/in., for the load increment from 87.5 to 88.75% of the experimental fracture load, to 2.99×10^1 lb/in. for the increment from 88.75 to 90%. Therefore, the failure strength becomes the stress at 88.75% or 26.20 ksi. This is below the actual fracture strength by 11%. For the instability analysis, there is not an upper bound since the elastic-load-displacement diagram remains linear.

The last method that can be used to predict fracture strength is the applied-load-vs-load-bearing-area (P-A_{LB}) diagram. The values of the applied load and the remaining load-bearing-area data are shown in Table 6.

The P-A_{LB} diagram is shown in Fig. 11. The values along the horizontal axis correspond to values of A_{LB} which is the load-bearing area of the plate between the notch and the edge of the plate. The load-bearing area represents the portion of the plate in which all laminae have not failed. The vertical axis values are the applied loads P. The straight line running in an oblique direction from the origin represents the boundary between loads and load-bearing areas that do not result in failure and those combinations that cause failure. Thus, the stress represented by any curve is equal to the unnotched tensile strength of 54.4 ksi when that curve crosses this oblique line.

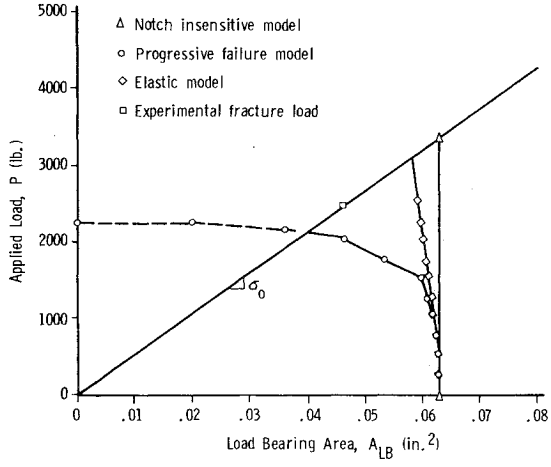

Fig. 11 Analytical-load vs load-bearing-area diagram for this specimen.

In order to explain the significance of the points on this diagram, the effect of notch sensitivity is examined. If the plate is not notch sensitive, the plate would fail when the load per area exceeded the unnotched tensile strength. The failure line would extend parallel to the load axis, and the failure load would be 3400 lb. Since the plate is notch sensitive, the failure load is less, 2530 lb. This is a 34% error.

The growth of a damage zone at the crack tip accounts for the notch sensitivity. The elastic analysis can be used to model damage zone growth as shown in the diagram. Using only the elastic analysis, the predicted fracture load is 3100 lb. This is a 23% error. As expected, the elastic analysis provides a prediction that is above the actual fracture load.

The progressive failure analysis can also be used to predict fracture strength. The failure curve using this analysis becomes nonlinear in the upper load levels as the damage zone growth accelerates. The predicted fracture load using the progressive failure analysis is 2110 lb. This prediction is 16% below the actual fracture strength. As predicted, using only theoretical considerations, the progressive failure analysis provides a lower bound on the fracture strength.

Conclusions

Using numerical models, it was possible to correlate ply subcrack length and K_I. Although it was not shown that the subcrack length was related to ultimate failure, the linear relation between $(K_I)^2$ and subcrack length does indicate that some principles of linear fracture mechanics do apply, at least in the immediate vicinity of the crack tip.

Through numerical modeling, it was also possible to bound the fracture strength for the center-notch specimen, using either K_I or one of the other models. Although the instability analysis provided the closest approximation of fracture strength, it did not provide an upper bound. The P-A_{LB} approach provided bounds that were as close to the actual strength as that calculated using K_I values. Since the P-A_{LB} approach is flexible, it is considered the better of three methods examined. Before this method can be applied to other laminates and structures, further research is required.

The numerical model presented in this paper is crude and could obviously be improved upon. The most important area requiring improvement is that of the strength criterion. A better criterion could possibly give better estimates of which element plies have failed. The next area requiring improvement is in the treatment of element stiffness after failure. The method presented herein always provides a lower bound solution which is important when considering problems in which experimental data are nonexistent or the experiment is in the planning stage. Improving stiffness characteristics may not provide a closer, conservative result. The last procedure that requires improvement is in the method of loading. Through the use of more sophisticated incremental loading and convergence methods, associated with nonlinear analysis, the predictions could be improved.

The applicability of the finite-element method in analyzing composite fracture has been shown for this special case. Since finite-element models can be applied to complicated structures and are not as costly as experimentation, further study into the application of finite elements to this type of problem is necessary and should prove profitable.

References

[1] Mandell, J. F., Wang, S. S., and McGarry, F. J., "Fracture of Graphite Fiber Reinforced Composites," Technical Rept. AFML-TR-73-142, Air Force Materials Laboratory, Wright-Patterson AFB, Ohio, July 1973.

[2] Tsai, S. W. and Hahn, H. T., "Recent Developments in Fracture of Filamentary Composites," *Proceedings of an International Conference on Prospects of Fracture Mechanics*, Woodhoff International, New York, N.Y., 1974, pp. 493-501.

[3]Hahn, H. T., "Fracture Behavior of Composite Laminates," presented at the International Conference on Fracture Mechanics and Technology, Hong Kong, March 21-25, 1977.

[4]Wu, E. M. and Reuter, R. C., Jr., "Crack Extension in Fiberglass Reinforced Plastics," T & AM Rept. 725, Urbana, Ill., Feb. 1965.

[5]Wu, E. M., "Fracture Mechanics of Anisotropic Plates," *Composte Materials Workshop*, edited by S. W. Tsai, J. C. Halpin, and N. J. Pagano, Technomic Publishing, Stamford, Conn., 1968.

[6]Morris, D. H. and Hahn, H. T., "Mixed Mode Fracture of Graphite/Epoxy Composites: Fracture Strength," *Journal of Composite Materials*, Vol. 11, April 1977, pp. 129-138.

[7]Morris, D. H. and Hahn, H. T., "Fracture Resistance Characterization of Graphite/Epoxy Composites," ASTM STP 617, presented at the ASTM 4th National Conference on Composite Materials: Testing and Design, Valley Forge, Penn., May 1976.

[8]Chang, F. H., Gordon, D. E., Rodini, B. T., and McDaniel, R. H., "Real Time Characterization of Damage Growth in Graphite/Epoxy Laminates," *Journal of Composite Materials*, Vol. 10, July 1976, pp. 182-192.

[9]Jones, R. M., *Mechanics of Composite Materials*, Scripto, Washington, D.C., 1975.

[10]Whitney, J. M. and Kim, R. Y., "Effect of Stacking Sequence on the Notched Strength of Laminated Composites," presented at the ASTM 4th National Conference on Composite Materials: Testing and Design, Valley Forge, Penn., May 1976.

[11]Hill, R., *The Mathematical Theory of Plasticity*, Oxford University Press, London, 1950.

[12]Tsai, S. W., "Strength Characteristics of Composite Materials," NASA Contractor Rept. CR-224, April 1965.

[13]Coffin, M. D. and Tiffany, C. F., "New Air Force Requirements for Structural Safety, Durability, and Lift Management," AIAA Paper 75-781, 1975.

[14]Phillips, D. C., "The Fracture Mechanics of Carbon Fibre Laminates," *Journal of Composite Materials*, Vol. 8, April 1974, pp. 130-141.

[15]Nuismer, R. J. and Whitney, J. M., "Uniaxial Failure of Composite Laminates Containing Stress Concentrations," *Fracture Mechanics of Composites*, American Society for Testing and Materials, Special Technical Publication 593, 1975.

[16]Venkayya, V. B. and V. A. Tischler, "Analyze-Analysis of Aerospace Structures with Member Elements," Technical Memorandum AFFDL-TM-FBR-78-89, Air Force Flight Dynamics Laboratory, Wright-Patterson AFB, Ohio, Aug. 1978.

[17]Chan, S. K., Tuba, J. S., and Witson, W. K., "On the Finite Element Method in Linear Fracture Mechanics," *Engineering Fracture Mechanics*, Vol. 2, Jan. 1970, pp. 1-7.

[18]Chou, S. C., Orringer, O., and Rainey, J. H., "Post-Failure Behavior of Laminates: I—No Stress Concentration," *Journal of Composite Materials*, Vol. 10, Oct. 1976, pp. 371-381.

[19]Chou, S. C., Orringer, O., and Rainey, J. H., "Post-Failure Behavior of Laminates: II—Stress Concentration," *Journal of Composite Materials*, Vol. 11, Jan. 1977, pp. 71-78.

[20]Yamada, Y. and Yoshimura, N., "Plastic Stress-Strain Matrix and Its Application for the Solution of Elastic-Plastic Problems by the Finite Element Method," *International Journal of Mechanical Sciences*, Vol. 10, May 1968, pp. 343-354.